

Higher-order corrections to the eikonal phase shifts for heavy-ion elastic collision

Moon Hoe Cha

Department of Physics, Kangwon National University, Chunchon 200-701, Republic of Korea

Yong Joo Kim

Department of Physics, Cheju National University, Cheju 690-756, Republic of Korea

(Received 30 August 1994)

We present first- and second-order corrections to the eikonal phase shifts for heavy-ion elastic scattering based on Coulomb trajectories of colliding nuclei. Including the first- and second-order corrections improves the agreement with the experimental data and the optical model result for the elastic scatterings in the $^{16}\text{O}+^{40}\text{Ca}$ and $^{16}\text{O}+^{90}\text{Zr}$ systems at $E_{\text{lab}}=1503$ MeV.

PACS number(s): 25.70.-z, 24.10.Ht

I. INTRODUCTION

There has been a great deal of effort [1-6] in describing scattering processes between heavy ions within the framework of the eikonal approximation method. In general, the eikonal scattering wave functions and phase shifts are derived from the Lipmann-Schwinger equation by a linearization of the Green's function in momentum space or from the integral equation by further approximating the WKB results [1,2]. The physical assumption of the eikonal approximation is that the energy of a projectile is sufficiently high that its classical trajectory is little deflected from a straight line.

The eikonal approximation has been found to be a very effective approach to high-energy potential scattering and has been applied to the scattering of hadrons by nuclei [7]. Recently, the Glauber model with first- and second-order noneikonal corrections has been applied to elastic nuclear scattering at intermediate energies by Fäldt *et al.* [5]. Carstoiu and Lombard [6] investigated the limitations of the eikonal approximation in the low-energy regime for the calculation of total and total reaction cross sections. They considered only light elements, neglecting the Coulomb phase. So far, the higher-order corrections to eikonal phase shifts are expressed in terms of the impact parameters $b = \sqrt{l(l+1)}/k$ and they have only been applied to the scattering of hadrons or light elements by nuclei.

In this paper we modify the eikonal phase shifts to include the deflection effect due to the Coulomb field and we also apply the modified eikonal phase shifts to elastic

scattering between heavy ions. In Sec. II we describe the formulation of the eikonal phase shifts based on the Coulomb trajectories of the colliding nuclei. Section III is devoted to an application of the present model for the systems $^{16}\text{O}+^{40}\text{Ca}$ and $^{16}\text{O}+^{90}\text{Zr}$ at $E_{\text{lab}}=1503$ MeV.

II. FORMALISM

If there is a single turning point in the radial Schrödinger equation, the WKB phase shifts are given by

$$\delta_l^{\text{WKB}} = \int_{r_t}^{\infty} k_l(r) dr - \int_b^{\infty} k \left[1 - \frac{b^2}{r^2} \right]^{1/2} dr, \quad (1)$$

where r_t is the turning point corresponding to the local wave number $k_l(r)$,

$$k_l(r) = k \left\{ 1 - \left[\frac{2\eta}{kr} + \frac{b^2}{r^2} + \frac{V_N(r)}{E} \right] \right\}^{1/2}, \quad (2)$$

where $k = \sqrt{2\mu E}/\hbar$, η is the Sommerfeld parameter, and $V_N(r)$ the nuclear potential. Wallace [8,9] expanded the solution of Eq. (1) in a power series in the strength of the potential in terms of the impact parameters b ,

$$\delta_l^{\text{WKB}} = \sum_{n=0}^{\infty} \delta_l^n, \quad (3)$$

where

$$\delta_{l=(kb-\frac{1}{2})}^n = -\frac{k[\mu/(\hbar k)^2]^{n+1}}{(n+1)!b^{2n}} \left[b^2 \left(1 + b \frac{d}{db} \right) \right]^n \int_0^{\infty} V^{n+1} [(b^2 + z^2)^{1/2}] dz. \quad (4)$$

Instead of Eq. (1), now we use the WKB expression for the nuclear elastic phase shifts, taking into account the deflection effect due to the Coulomb field [10-12],

$$\delta_l^{\text{WKB}} = \int_{r_t}^{\infty} k_l(r) dr - \int_{r_c}^{\infty} k_c(r) dr, \quad (5)$$

where

$$r_c = \frac{\eta}{k} + \left[\left(\frac{\eta}{k} \right)^2 + b^2 \right]^{1/2} \quad (6)$$

and

$$k_c(r) = k \left[1 - \left(\frac{2\eta}{kr} + \frac{b^2}{r^2} \right) \right]^{1/2}. \quad (7)$$

Then Eq. (4) can further be written in terms of r_c as follows:

$$\delta_{l=(kr_c-\frac{1}{2})}^n = -\frac{k[\mu/(\hbar k)]^{2n+1}}{(n+1)!r_c^{2n}} \left[r_c^2 \left(1 + r_c \frac{d}{dr_c} \right) \right]^n \int_0^\infty V_N^{n+1} [(r_c^2 + z^2)^{1/2}] dz. \quad (8)$$

Expressions for the first three terms in this equation are explicitly

$$\delta_l^0 = -\frac{\mu}{\hbar^2 k} \int_0^\infty V_N(\sqrt{r_c^2 + z^2}) dz, \quad (9a)$$

$$\delta_l^1 = -\frac{\mu^2}{2\hbar^4 k^3} \left(1 + r_c \frac{d}{dr_c} \right) \int_0^\infty V_N^2(\sqrt{r_c^2 + z^2}) dz, \quad (9b)$$

$$\delta_l^2 = -\frac{\mu^3}{6\hbar^6 k^5} \left(3 + 5r_c \frac{d}{dr_c} + r_c^2 \frac{d^2}{dr_c^2} \right) \int_0^\infty V_N^3(\sqrt{r_c^2 + z^2}) dz. \quad (9c)$$

The Coulomb-modified eikonal phase shifts in Eqs. (9a)–(9c) have the same forms as the eikonal expressions with impact parameters b by Wallace. Instead of b , however, we obtained the expressions of the Coulomb-modified eikonal phase shifts in terms of the distance of closest approach, r_c , due to the deflection effect of the Coulomb field. By taking $V_N(r)$ as the optical Woods-Saxon potential given by

$$V_N(r) = -\frac{V_0}{1 + e^{(r-R_v)/a_v}} - i\frac{W_0}{1 + e^{(r-R_w)/a_w}}, \quad (10)$$

we can use the three eikonal phase shifts in the general expression for the elastic scattering amplitude. The elastic scattering cross sections are then obtained from the scattering amplitude

$$f(\theta) = f_R(\theta) + \frac{1}{ik} \sum_{l=0}^{\infty} \left(l + \frac{1}{2} \right) e^{2i\sigma_l} (S_l - 1) P_l(\cos \theta), \quad (11)$$

where $f_R(\theta)$ is the usual Rutherford scattering amplitude and σ_l the Coulomb phase shift. The S -matrix elements S_l in this equation can be expressed by the nuclear phase shifts δ_l as

$$S_l = e^{2i\delta_l}. \quad (12)$$

Since the nuclear phase shifts are complex, the variations of the Coulomb and real parts of the nuclear phase shifts

over l give the deflection function

$$\theta_l = 2\frac{d}{dl}(\sigma_l + \text{Re } \delta_l). \quad (13)$$

This deflection angle is a semiclassical treatment of a trajectory with angular momentum l .

III. RESULTS AND CONCLUSIONS

As in the preceding section, we have calculated the elastic differential cross sections for $^{16}\text{O}+^{40}\text{Ca}$ and $^{16}\text{O}+^{90}\text{Zr}$ systems at $E_{\text{lab}}=1503$ MeV by using the Coulomb-modified eikonal phase shift and its two higher-order corrections. Parameters of the Woods-Saxon potential are given in Table I. In Fig. 1, the short-dashed curve is the result for the zero-order eikonal phase shifts, while the dotted and solid curves are the results for the first- and second-order corrections. As seen in this figure, the differences between the short-dashed and dotted and solid curves are substantial when compared to the experimental results of Ref. [13]. Furthermore, these differences give some variations in the depths of the minimum and a change in the location of the minimum. However, the differences between the results from the first- and second-order corrections are too small so that the dotted curves overlap with the solid curves. As a whole, we can find in Fig. 1 that the two results calculated from the first- and second-order corrections improve the agree-

TABLE I. Parameters of the fitted Woods-Saxon potential for ^{16}O beams at $E_{\text{lab}}=1503$ MeV. Values are taken from Ref. [13].

System	V_0 (MeV)	r_v (fm)	a_v (fm)	W_0 (MeV)	r_w (fm)	a_w (fm)
$^{16}\text{O}+^{40}\text{Ca}$	60.0	1.042	0.710	54.1	1.042	0.710
$^{16}\text{O}+^{90}\text{Zr}$	129.0	0.946	0.790	124.1	0.946	0.790

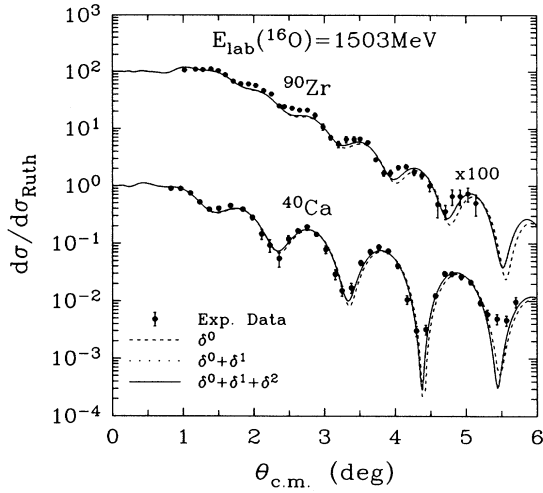


FIG. 1. Elastic scattering angular distributions for $^{16}\text{O}+^{40}\text{Ca}$ and $^{16}\text{O}+^{90}\text{Zr}$ systems at $E_{\text{lab}}=1503$ MeV. The solid circles denote the observed data taken from Ref. [13].

ment with the observed data for $^{16}\text{O}+^{40}\text{Ca}$ and $^{16}\text{O}+^{90}\text{Zr}$ systems at $E_{\text{lab}}=1503$ MeV compared to the result of the zero-order eikonal phase shifts.

The transmission functions $T_l = 1 - |S_l|^2$ and deflection functions θ_l are plotted in Figs. 2 and 3. Figures 2(a) and 2(b) show the transmission and deflection functions corresponding to the potential for $^{16}\text{O}+^{40}\text{Ca}$ system at $E_{\text{lab}}=1503$ MeV, while Figs. 3(a) and 3(b) show those two functions for $^{16}\text{O}+^{90}\text{Zr}$ at $E_{\text{lab}}=1503$ MeV. The deflection functions in these figures have two typical extreme values. One is the nuclear rainbow associated with the maximum negative deflection angle due to a nuclear attraction; the other is the Coulomb rainbow associated with the maximum positive angle due to a Coulomb repulsion. In Fig. 2(b), we can see that the nuclear rainbow of the second-order corrections is slightly moved toward the right compared to the result of zero-order phases, while the Coulomb rainbow has the same position and magnitude. We can also notice in Fig. 3(b) that the deflection function for $^{16}\text{O}+^{90}\text{Zr}$ has a similar structure as the case for $^{16}\text{O}+^{40}\text{Ca}$, but the magnitudes of the nuclear and Coulomb rainbow angles for $^{16}\text{O}+^{90}\text{Zr}$ are somewhat larger than the results for $^{16}\text{O}+^{40}\text{Ca}$.

A further investigation of the situation can be gained by looking at the transmission functions. In Figs. 2(a) and 3(a), we can see in both cases that the transmission functions of the second-order corrections are shifted toward the right compared with those of the zero-order eikonal phases. Such shifts compensate the values of transmission function underestimated in the zero-order eikonal phases. Those shifts are also reflected in the reac-

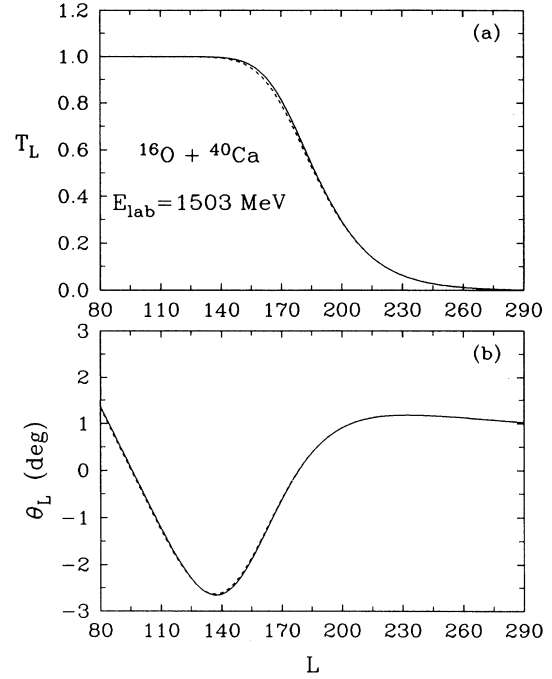


FIG. 2. Transmission and deflection functions for the system $^{16}\text{O}+^{40}\text{Ca}$ at $E_{\text{lab}}=1503$ MeV plotted versus angular momentum L . The short-dashed and solid curves correspond to the transmission and deflection functions with the zero-order eikonal phase shift and its second-order correction, respectively.

tion cross sections as displayed in Table II. We can notice in this table that the agreement of the results from the first- and second-order corrected phases are satisfactorily good (relative discrepancy=0.4% for $^{16}\text{O}+^{40}\text{Ca}$ and 1.0% for $^{16}\text{O}+^{90}\text{Zr}$) with the optical model result compared to the result of the zero-order eikonal phases.

The near- and far-side decompositions [14] of the scattering amplitudes with the second-order corrections to the eikonal phase shifts were also performed by replacing the associated polynomials $P_{lm}(\cos\theta)$ by

$$Q_{lm}^{\pm}(\cos\theta) = \frac{1}{2}[P_{lm}(\cos\theta) \mp i(2/\pi)Q_{lm}(\cos\theta)], \quad (14)$$

where Q_{lm} is a Legendre function of the second kind. The contributions of the near- and far-side components to elastic scattering cross sections are shown in Fig. 4 along with the total differential cross section. The total differential cross section is not just a sum of the near- and far-side cross sections but contains the interference between near- and far-side amplitudes as seen in Fig. 4. The refraction oscillations observed on the elastic scattering cross section of $^{16}\text{O}+^{40}\text{Ca}$ system are due to the

TABLE II. Comparison of the reaction cross sections (in mb) obtained from the first-order (Cal. 2) and second-order corrections (Cal. 3) to the zero-order eikonal phase shifts (Cal. 1) with respect to the optical model result. Values with optical model are taken from Ref. [13].

System	Cal. 1	Cal. 2	Cal. 3	Optical model
$^{16}\text{O}+^{40}\text{Ca}$	1966	1980	1981	1996
$^{16}\text{O}+^{90}\text{Zr}$	2707	2722	2723	2749

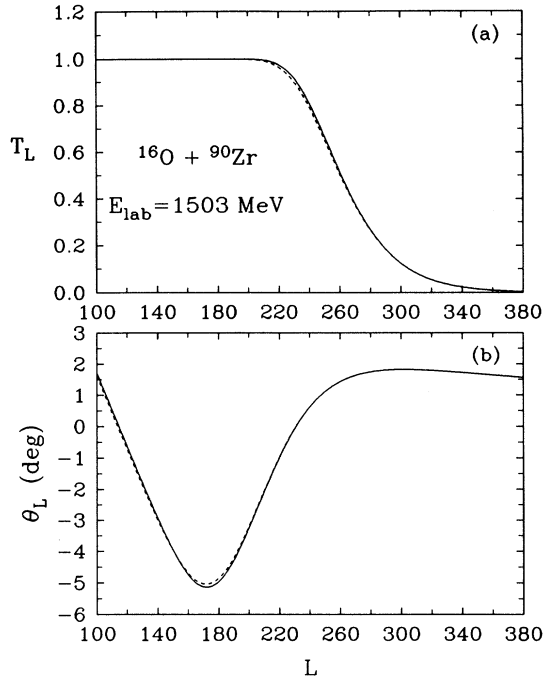


FIG. 3. Transmission and deflection functions for the system $^{16}\text{O}+^{90}\text{Zr}$ at $E_{\text{lab}}=1503$ MeV plotted versus angular momentum L . The short-dashed and solid curves correspond to the transmission and deflection functions with the zero-order eikonal phase shift and its second-order correction, respectively.

strong interference between the near- and far-side components. The magnitudes of the near- and far-side contributions are about the same around 4.7° ; however, the far-side dominates at angles greater than this. On the other hand, in case of $^{16}\text{O}+^{90}\text{Zr}$ elastic scattering, the far-side component becomes very small compared with the near-side one over the whole angle. Because of the smallness of the far amplitude, we can see that the cross sections of the $^{16}\text{O}+^{90}\text{Zr}$ system show weak oscillations.

In conclusion, we have presented the first- and second-order corrections to the zero-order eikonal phase shifts based on the Coulomb trajectory of the colliding nuclei. We have found that the differential and total reaction cross sections calculated from the first- and second-order eikonal phase shifts improve the agreement with the experimental data and optical model result for $^{16}\text{O}+^{40}\text{Ca}$ and $^{12}\text{C}+^{90}\text{Zr}$ systems at $E_{\text{lab}}=420$ MeV, respectively, compared to the result of the zero-order phases. However, we have found that the differences between the first- and second-order corrections to the zero-order eikonal phase shifts are too small. We have also found that the transmission functions and nuclear rainbows of the second-order eikonal corrections for the $^{16}\text{O}+^{40}\text{Ca}$ and

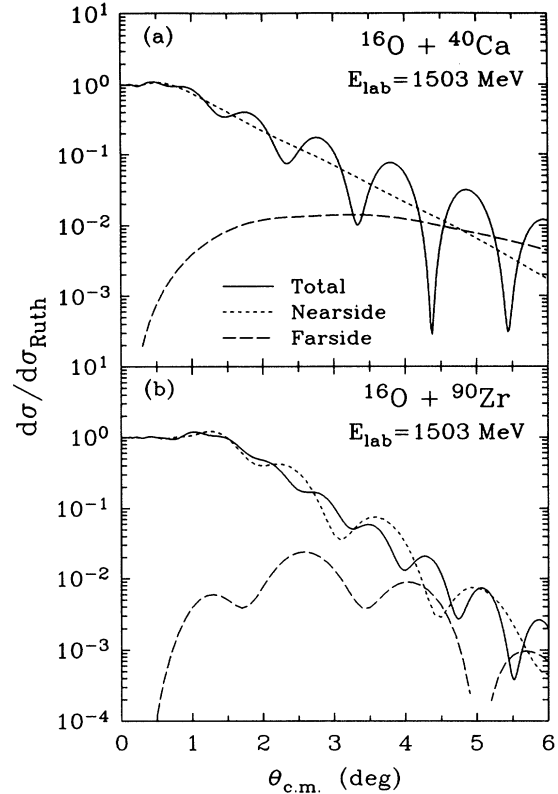


FIG. 4. Differential cross sections (solid curves), near-side contributions (short-dashed curves), and far-side contributions (long-dashed curves) following Fuller's formalism [14] by using the second-order corrections to the eikonal phase shifts for the systems (a) $^{16}\text{O}+^{40}\text{Ca}$ and (b) $^{16}\text{O}+^{90}\text{Zr}$ at $E_{\text{lab}}=1503$ MeV.

$^{12}\text{C}+^{90}\text{Zr}$ systems were moved toward the right compared to the results of the zero-order eikonal phases, while the Coulomb rainbows did not change their positions and magnitudes in both cases. The shifts of the transmission functions have been reflected in the reaction cross sections. Through near- and far-side decompositions of the cross section we have also shown that the refraction oscillations of the $^{16}\text{O}+^{40}\text{Ca}$ system are due to the strong interference between the near- and far-side amplitudes, and the near-side one dominates for the $^{16}\text{O}+^{90}\text{Zr}$ system.

ACKNOWLEDGMENTS

It is a great pleasure to thank Dr. N. Alamanos and his colleagues for providing us with their experimental data. The present study was supported in part by the Ministry of Education, Korea (Project No. BSRI-94-2402).

- [1] T. W. Donnelly, J. Dubach, and J. D. Walecka, Nucl. Phys. **A232**, 355 (1974).
 [2] J. Knoll and R. Schaeffer, Ann. Phys. (N.Y.) **97**, 307 (1976).

- [3] J. Chauvin, D. Lebrun, F. Durand, and M. Buenerd, J. Phys. G **11**, 261 (1985).
 [4] R. da Silveira and Ch. Leclercq-Willain, J. Phys. G **13**, 149 (1987).

- [5] G. Fäldt, A. Ingemarsson, and J. Mahalanabis, *Phys. Rev. C* **46**, 1974 (1992).
- [6] F. Carstoiu and R. J. Lombard, *Phys. Rev. C* **48**, 830 (1993).
- [7] D. Waxman, C. Wilkin, J.-F. Fermond, and R. J. Lombard, *Phys. Rev. C* **24**, 578 (1981).
- [8] S. J. Wallace, *Ann. Phys. (N.Y.)* **78**, 190 (1973).
- [9] S. J. Wallace, *Phys. Rev. D* **8**, 1846 (1973).
- [10] S. Landowne, C. H. Dasso, B. S. Nilsson, R. A. Broglia, and A. Winther, *Nucl. Phys.* **A259**, 99 (1976).
- [11] C. K. Chan, P. Suebka, and P. Lu P, *Phys. Rev. C* **24**, 2035 (1981).
- [12] D. M. Brink, *Semi-Classical Methods for Nucleus-Nucleus Scattering* (Cambridge University Press, Cambridge, England, 1985), p. 37.
- [13] P. Roussel-Chomaz, N. Alamanos, F. Auger, J. Barrette, B. Berthier, B. Fernandez, and L. Papineau, *Nucl. Phys.* **A477**, 345 (1988).
- [14] R. C. Fuller, *Phys. Rev. C* **12**, 1561 (1975).